Solution Structure of Human β-Parvalbumin and Structural Comparison with Its Paralog α-Parvalbumin and with Their Rat Orthologs[†,‡]

Elena Babini,[§,||] Ivano Bertini,*[,§,⊥] Francesco Capozzi,[§,||] Cristina Del Bianco,[§,⊥] Dominik Hollender,[§,@,○] Tamas Kiss,[@] Claudio Luchinat,[§,#] and Alessandro Quattrone[§,+]

CERM, Via Luigi Sacconi 6, 50019 Sesto Fiorentino, Italy, Department of Food Science, University of Bologna, via Ravennate 1020, 47023 Cesena, Forlì, Italy, Department of Chemistry, University of Florence, Via Luigi Sacconi 6, 50019 Sesto Fiorentino, Italy, Department of Inorganic and Analytical Chemistry, University of Szeged, Szeged, Hungary, Department of Agricultural Biotechnology, University of Florence, P.le delle Cascine 28, 50144 Florence, Italy, and FiorGen Foundation, Via Luigi Sacconi 6, 50019 Sesto Fiorentino, Italy

Received July 28, 2004; Revised Manuscript Received October 19, 2004

ABSTRACT: The aim of this research was to determine the structure of human β-parvalbumin (109 amino acids) and to compare it with its paralog and ortholog proteins. The structure was determined in solution using multinuclear and multidimensional NMR methods and refined using substitution of the EF-hand Ca^{2+} ion with a paramagnetic lanthanide. The resulting family of structures had a backbone rmsd of 0.50 Å. Comparison with rat oncomodulin (X-ray, 1.3 Å resolution) as well as with human (NMR, backbone rmsd of 0.49 Å) and rat (X-ray, 2.0 Å resolution) parvalbumins reveals small but reliable local differences, often but not always related to amino acid variability. The analysis of these structures has led us to propose an explanation for the different affinity for Ca^{2+} between α- and β-parvalbumins and between parvalbumins and calmodulins.

Parvalbumins are small (∼11.5 kDa) Ca^{2+}-binding proteins belonging to a protein superfamily called EF-hand by the name of the most common Ca^{2+}-binding domain in vertebrate genomes. Parvalbumins arose in vertebrates as two sublineages, termed α and β (*1*), with only one member each present in mammals. Even if α- and β-parvalbumin, the latter also known as oncomodulin, display the same basic domain architecture and are encoded by close paralog genes with similar exon−intron arrangements (*2*), they substantially differ in the pattern of expression and in their Ca^{2+} binding properties. Therefore, they could be endowed with divergent functional roles.

α-Parvalbumin is expressed mainly in fast-twitch skeletal myofibrils (*3*), where it is abundant, and GABAergic neurons (*4*), while oncomodulin was originally identified in rat hepatomas (*5*) and subsequently detected in the blastocyst and the cytotrophoblasts of the placenta (*6*). Its presence in solid tumors has also been confirmed in *in vitro* models of chemical and viral carcinogenesis (*7*, *8*), and by the immunohistochemical analysis of a number of human neoplastic tissues and primary or immortalized cell lines (*9*), with the recent evidence of a selective overexpression in rat mammary and pancreatic adenocarcinomas (*10*). The term oncomodulin has therefore been derived from its consideration as an oncofetal protein, since it is completely absent in a variety of normal mammalian tissues (*11*). More recently, however, oncomodulin has been found to be expressed in a very specialized district, the cochlear outer hair cells of the organ of Corti, the basic structure of the mammalian auditory system (*12*).

Parvalbumins have been ascribed to the category of EF-hand-containing Ca^{2+}-buffering proteins, as opposed to the Ca^{2+}-sensor proteins whose prototype is calmodulin. Both α-parvalbumin and oncomodulin are endowed with three consecutive EF-hand domains, each characterized by the consensus arrangement of two α-helices linked by a Ca^{2+}-coordinating loop in a pentagonal bipyramidal configuration, originally termed the AB, CD, and EF helices [it is indeed from the C-terminal EF segment of carp parvalbumin that the EF-hand domain derived its name three decades ago (*13*)]. This overall homogeneous arrangement hides substantial differences. The AB site of both parvalbumins is a nonfunctional, vestigial EF-hand due to the absence of oxygen-bearing residues at critical positions in the central loop (*14*). It is endowed with the interesting structural property of being associated with the hydrophobic sides of the paired CD and EF sites (*15*) because its antiparallel helix−loop−helix arrangement forms a plate with one polar and one hydrophobic side, the latter filling the hydrophobic

[†] This research was financially supported under EU Contract QLG2-CT-2002-0098 (SPINE), Ente Cassa di Risparmio di Firenze, and Fondo per gli investimenti della ricerca di base (MIUR), Contract RBNE01TTJW.

[‡] Atomic coordinates and NMR restraints have been deposited in the Protein Data Bank as entry 1TTX.

* To whom correspondence should be addressed: Magnetic Resonance Center (CERM) and Department of Chemistry, University of Florence, Via Luigi Sacconi, 6, 50019 Sesto Fiorentino, Italy. Telephone: +390554574272. Fax: +390554574271. E-mail: ivanobertini@cerm.unifi.it.

[§] CERM.

[||] University of Bologna.

[⊥] Department of Chemistry, University of Florence.

[@] University of Szeged.

[○] Permanent address: University of Szeged.

[#] Department of Agricultural Biotechnology, University of Florence.

[+] FiorGen Foundation.

10.1021/bi048388o CCC: $27.50
Published on Web 12/04/2004

basket formed by the CD and EF domains. In α-parvalbumins, these EF-hands exhibit a K_d of $<10^{-7}$ M for Ca^{2+} while being able to bind Mg^{2+} ($K_d < 10^{-4}$ M) (*16*−*18*). Since high-affinity EF-hands tend to be permanently occupied by Ca^{2+} ions under physiological conditions, they are well-suited to serving structural and Ca^{2+} buffering roles.

Interestingly, the CD site of rat oncomodulin, having a K_d for Ca^{2+} of $\sim10^{-6}$ M and a K_d for Mg^{2+} of $>10^{-3}$ M (*19*), has to be ascribed to the other category of EF-hands with respect to Ca^{2+} affinity, that of low-affinity sites, unoccupied at basal intracellular Ca^{2+} concentrations, which undergo conformational change with Ca^{2+} binding following the increase in cytosolic Ca^{2+} levels. This change is typical of Ca^{2+}-sensing proteins, which expose effector binding sites and perform regulatory roles.

Although, taken together, these observations are consistent with a regulatory function of oncomodulin, no effector protein has been identified to date, and no convincing biochemical regulatory activity has been demonstrated for oncomodulin, despite some early proposals (*20*−*22*).

In an attempt to gain further clues that would be useful in solving the problem of the opposing putative buffer/sensing functions of this interesting Ca^{2+}-binding protein, in this paper, we present the solution structure of human Ca^{2+}-loaded oncomodulin as determined by NMR[1] spectroscopy. The available structure of human α-parvalbumin (*23*), obtained previously by our group with the same experimental approach, allows a detailed comparison of the structural features of the two proteins and of their potential Ca^{2+} binding properties. A further comparison with the X-ray structures of rat α- and *β*-parvalbumins (*24*, *25*) is also reported.

Altogether, the structural data presented and the comparisons we have performed with the rat orthologs suggest an interpretation which could explain the high differential affinity for Ca^{2+} and Mg^{2+} of the two parvalbumins in the absence of marked conformational differences, and which could also indicate that indeed both proteins are evolutionarily "degenerated" versions of true Ca^{2+}-sensing proteins. Following this perspective, this work adds a structural rationale to a signaling role for oncomodulin, which is also more consistent with a specialized physiological activity of this protein in the mammalian auditory system and with a perturbation of signal transduction events by its unscheduled expression during oncogenesis.

MATERIALS AND METHODS

Gene Cloning. The gene encoding human oncomodulin was amplified by PCR starting from human cerebellar cDNA, using the following oligonucleotides as primers: upper strand from 5′ to 3′, ATGAGCATCACGGACGTG; and lower strand from 5′ to 3′, CGCGTTAAGAATGCACCA.

Amplification was carried out using the thermostable PfuI polymerase (Stratagene) to reduce the error rate and the addition of non-template-directed nucleotides at the 3′ end of the PCR-generated fragment. The blunt-ended oncomodulin cDNA from PCR amplification was purified from an agarose gel, phosphorylated, and then cloned into the StuI site of the multiple cloning site of plasmid pQE30Xa (Qiagen) by blunt-end ligation. The pQE30Xa expression plasmid is designed for expression of His-tagged proteins. The "Quick ligation kit" (New England Biolabs) was used to maximize the yield of the ligation reaction which was then transformed into supercompetent Xl1Blue cells (Novagen). The colonies obtained on LB (with ampicillin) plates were screened for protein expression.

Plasmids from bacterial colonies expressing a protein of the correct molecular mass were purified and sequenced.

All the samples that were sequenced contained a single nucleotide variation with respect to the reference NM_006188 GenBank sequence for human oncomodulin at position 59. This variation changes the second nucleotide of the CAA codon, encoding glutamine at position 19, to the CGA codon, encoding arginine. Inspection of the dbSNP database revealed that the transition from A to G at position 59 of the oncomodulin cDNA is recorded as the only nonsynonymous single-nucleotide polymorphism present, annotated with unvalidated status and unknown allele frequency (SNP entry rs13312633). Therefore, our recombinant oncomodulin sequence is very likely a true allelic variant of the reference oncomodulin gene, and not an artifact or a mutation.

Protein Purification. Recombinant His-tagged human [^{15}N]-oncomodulin was purified from *Escherichia coli* Xl1Blue grown in 2 L of minimal medium (MM) containing [^{15}N]-ammonium sulfate as the nitrogen source. The ^{13}C- and ^{15}N-labeled protein sample was obtained using the same medium, but replacing [^{12}C]glucose with [^{13}C]glucose. The cells from 2 L of LB culture in the exponential growth phase (A_{600} = 0.5/0.6) were collected by centrifugation at 8000 rpm, rinsed with 20 mL of MM, and centrifuged again, to remove any amount of rich medium. The pellet was resuspended in 10 mL of MM and transferred to 2 L of MM containing 0.2% glucose (preculture/final volume ratio = 1/1). IPTG was used to induce protein expression and was added to the culture 2.5 h after incubation. Incubation of the preculture and final culture was carried out at 37 °C, shaking at 150 rpm for 15 h after induction.

Cells were collected from stationary-phase cultures (typically 15 h after induction with IPTG) by centrifugation at 8000 rpm, for 15 min, and resuspended in ∼25 mL of buffer 1 [20 mM Tris (pH 8.0), 1 mM $MgSO_4$, 1 mM $CaCl_2$, 100 mM KCl, DNase, and 1 mM PMSF]. Disruption of the cells was achieved by two passages through a French press (1000 psi). The lysate was then centrifuged at 14 000 rpm for 30 min, and the supernatant, containing the soluble recombinant protein, was loaded onto a 5 mL HiTRAP chelating column (Pharmacia), previously conditioned with buffer 2 [20 mM Tris (pH 8.0)]. After two washing steps with 50 mL of buffer 2 and 50 mL of buffer 3 [20 mM Tris (pH 8.0) and 300 mM KCl (pH 6.0)], elution of the protein was carried out in one step, using buffer 4 [20 mM Tris (pH 8.0) and 300 mM imidazole].

[1] Abbreviations: PV, α-parvalbumin; OM, oncomodulin (*β*-parvalbumin); CaM, calmodulin; NMR, nuclear magnetic resonance; IPTG, isopropyl *β*-D-thiogalactopyranoside; HSQC, heteronuclear single-quantum coherence; PCS, pseudocontact shifts; RDC, residual dipolar couplings; IPAP, in-phase/anti-phase; TAD, torsion angle dynamics; REM, restrained energy minimization; CaCaOM, dicalcium oncomodulin; CaTbOM, Tb^{3+}-substituted oncomodulin; CBCANH, C*β*−Cα−NH connectivity experiment; CBCACONH, C*β*−Cα−carbonyl carbon−NH connectivity experiment; NOESY, nuclear Overhauser effect spectroscopy; TOCSY, total correlation spectroscopy; TROSY, transverse-relaxation optimized spectroscopy; CSI, chemical shift index.

The protein was then dialyzed against buffer 5, for factor Xa [20 mM Tris (pH 8.0), 100 mM NaCl, and 1 mM $CaCl_2$], and concentrated to ~3 mL. Factor Xa was added to the protein (150 μg of enzyme/10 mg of protein), and the mixture was incubated at 23 °C for ~16 h under mild shaking to cleave the histidine tag. The tag and the uncut protein were removed from the mixture through a passage on the HiTRAP chelating column. Remaining contaminants were removed by gel filtration on a Superdex G-75 HiLoad column, at room temperature, in 0.1 M NaCl. The pH of the protein was adjusted to 6.0, and the sample was concentrated to the final volume of 0.5 mL.

Protein concentrations were determined spectrophotometrically, assuming $\epsilon_{274} = 3260\ M^{-1}\ cm^{-1}$ (*26*), and the purity was checked on polyacrylamide gel electrophoresis.

NMR Sample Preparation and Measurements. The NMR samples were prepared by dissolving the protein in 600 μL of an aqueous solution containing 100 mM NaCl and 10% D_2O. The pH was adjusted to 6.5 using 0.01 M NaOH or HCl solutions. The final concentrations of the singly and doubly labeled samples were around 4 mM.

The Tb^{3+}-substituted oncomodulin (CaTbOM) sample, with Tb^{3+} replacing the Ca^{2+} ion in the EF site, was prepared by titration of the dicalcium oncomodulin (CaCaOM), up to a Tb^{3+}/Ca^{2+} ratio of 0.9/1 to avoid occupancy of other sites.

The titration progress was followed by two-dimensional (2D) $^1H-^{15}N$ HSQC (*27*) spectra at 700 MHz. The achievement of the desired Tb^{3+}/Ca^{2+} ratio of 0.9/1 was monitored (*28*), as cross-peaks of the CaCaOM form disappeared, while the new signals of the CaTbOM complex developed their full intensity.

The NMR spectra were acquired on a Bruker AVANCE 700 spectrometer (700.13 MHz nominal proton frequency), and the R_1, R_2, and NOE relaxation measurements were taken at 283 and 298 K using a Bruker AVANCE 600 spectrometer (600.13 MHz nominal proton frequency). Both spectrometers were equipped with a triple-resonance (TXI) 5 mm probe with a *z*-axis pulse field gradient. All spectra were recorded at 283 K. The water signal was suppressed using presaturation during the relaxation delay and mixing time or by using the WATERGATE (*29*) method. All NMR experiments are described in the Supporting Information.

The 2D spectra were processed with XWINNMR Bruker software, while the three-dimensional (3D) spectra were processed with NMRPipe (*30*). All spectra were analyzed by Sparky (University of California, San Francisco, CA) (*31*) using extensions written in python computer language.

To obtain PCS values of the native protein and Tb^{3+}-substituted derivative, $^1H-^{15}N$ HSQC spectra were recorded at 298 K using spectral widths of 14 and 38 ppm in the ^1H and ^{15}N dimensions, respectively; 256 increments each with 1024 complex data points and 48 transients were collected. Raw data were multiplied in both dimensions by a squared cosine window function and Fourier transformed to obtain a final matrix of 1024 × 1024, or 512 × 512 real data points for HSQC spectra. A polynomial baseline correction was applied in the f_2 dimension.

One-bond $^1H-^{15}N$ coupling constants were measured at 298 K and 700 MHz either by fitting a series of $^1J_{NH}$-modulated HSQC spectra (*32*) or by using the IPAP method (*33*).

The relaxation measurements were carried out by recording a series of $^1H-^{15}N$ HSQC spectra with flip-back (*34*) and phase sensitive pulse sequences (*35*). R_1 and R_2 were both measured with 10 different delays and a CPMG pulse sequence (*36*) with a refocusing delay, τ_m, of 450 μs for the R_2 measurements. R_1 and R_2 were calculated by fitting the peak heights versus delay time using a single-exponential decay according to the Levenberg−Marquardt equation (*37*, *38*). Uncertainties were determined by using a Monte Carlo approach (*39*). Heteronuclear $^1H-^{15}N$ NOEs were calculated by taking the ratio of peak volumes with and without ^1H saturation.

Structure Calculation. 3D NOESY-HSQC cross-peak volumes were determined with Sparky using Gaussian peak shapes. The validity of the integration results was tracked by checking the line width of each dimension. The integrals were converted to upper distance limits by CALIBA (*40*). Dihedral ϕ and ψ angles, stereospecific assignments, and H-bonds were the additional input constraints for structure calculations.

DYANA (*41*) employing torsion angle dynamics (TAD) combined with a simulated annealing algorithm was used to calculate a series of 200 structures in 10 000 annealing steps starting from randomly generated conformers.

The quality of each structure is described by the value of a target function that is proportional to the squared deviations of the calculated restraints from the experimental ones plus the squared van der Waals violations. The metal ions were introduced by a linker made of pseudoatoms to the C-terminus and were imposed to be between 2.0 and 2.8 Å from the donor atoms of the CD- and EF-hand (*42*−*44*). The PCS and RDC values for the Tb^{3+}-substituted derivative were used as paramagnetic restraints together with all diamagnetic restraints through the appropriate PARAMAGNETIC-DYANA modules (*45*). Tolerances of ±10% or ±0.10 ppm for the PCS values and ±0.50 Hz for RDC values were used for the structural calculation. A fixed weight of 0.5 for PCS and 0.1 for RDC values relative to the weight of 1 for the NOEs was used in the calculations.

The 20 structures with the lowest target function were included in the final set to determine the rmsd values from the mean for the backbone atoms and for all heavy atoms. MOLMOL (*46*) and PROCHECK (*47*) were subsequently used for secondary structure analysis. The final family of the 20 best structures was minimized by iterative cycles of PARAMAGNETIC-DYANA, coupled to the RAMADYANA module (*48*) followed by restrained energy minimization (REM) with AMBER 5.0 (*49*).

The coordinates have been deposited in the Protein Data Bank (PDB entry 1TTX).

RESULTS

The parallel analysis of CBCANH and CBCA(CO)NH (*50*) led to the backbone resonance assignment. One hundred three of 108 amide resonances were assigned in this way. The missing amino acids, two prolines, two glutamates, and one glutamine, were found later by analyzing the 3D NOESY-HSQC (*51*) spectrum.

The analysis of the HN(CA)CO and HNCO spectra (*50*) allowed us to assign the carbonyl resonances of the protein.

Furthermore, we detected 18 H-bonds in the TROSY-like HNCO spectra (*52*).

The aliphatic side chain spin systems were obtained through the 3D CC(CO)NH spectra (*53*) and (H)CCH-TOCSY spectra (*54*) and in some cases with the help of 3D NOESY-HSQC spectra. The assignment of the aromatic resonances was carried out by the analysis of 2D NOESY (*55*) and 2D TOCSY (*55*) spectra. The side chain NH_2 resonances of the glutamines and asparagines were assigned while analyzing the $^1H-^{15}N$ HSQC spectrum together with the 3D NOESY-HSQC spectra.

The backbone ϕ and ψ angles were estimated by the chemical shift index (CSI) (*56*). $^3J_{HNH\alpha}$ coupling constants were determined in the 600 MHz HNHA (*57*) experiment. Eight α-helices, whose position was identical with that of the corresponding helices of the rat oncomodulin, were predicted by CSI.

The ^1H, ^{15}N, and ^{13}C resonance assignments are in the Supporting Information. The assigned nuclei are 98, 93, and 96.5% for ^1H, ^{13}C, and ^{15}N, respectively.

NOE Restraints. The analysis of the ^{13}C-edited and ^{15}N edited 3D NOESY-HSQC spectra provided 2300 assigned cross-peaks and 1912 unique upper distance limits, of which 1708 were found to be meaningful. The meaningful constraints consisted of 160 intraresidue, 537 sequential, 640 medium-range, and 371 long-range NOEs. The plot of the meaningful NOEs per residue is shown in the Supporting Information. The average of the meaningful NOEs per residue is around 17; 31 stereospecific assignments were identified by GLOMSA (*40*). Distance restraints, dihedral angles, stereospecific assignments, and H-bonds were used for structure calculations (Table 1).

Pseudocontact Shifts. It is well-known, and here confirmed, that lanthanides occupy the C-terminal EF-hand loop of EF-hand domains in general and of parvalbumins in particular (*58*−*60*), without inducing structural perturbations outside the immediate vicinity of the metal ion (*61*). Tb^{3+} has been chosen as one of the lanthanides providing the largest PCS because we were interested in the refinement of the AB domain with the respect to the rest of the protein (*28*, *42*).

Tb^{3+} in CaTbOM broadens lines sometimes beyond detection; 74 (62 backbone NH and 12 side chain NH_2) of 88 detectable peaks in the $^1H-^{15}N$ HSQC spectrum of the Tb^{3+}-substituted protein (CaTbOM) were assigned in a semiautomated way using predictions based on the paramagnetic susceptibility anisotropy and the predicted structure as discussed elsewhere (*23*). The metal−nuclei distances and the ratios between ^1H and ^{15}N pseudocontact shifts were also taken into account during the assignment procedure. These ratios were considered to be in the range of 0.75−1.30 for all NH groups that are more than 12 Å from the metal.

The anisotropy tensor parameters were calculated using the PCS values of 14 $^1H-^{15}N$ HSQC peaks, by FANTASIA (*62*). The equation relating PCS and the magnetic anisotropy parameters is (*63*)

$$\mathrm{PCS} = \delta^{pc} = \frac{1}{12\pi r_i^3}\left[\Delta\chi_{ax}^{para}(3\cos^2\theta - 1) + \frac{3}{2}\Delta\chi_{rh}^{para}(\sin^2\theta\cos 2\Omega)\right] \quad (1)$$

Table 1: Type and Number of Restraints Used in the DYANA Calculation and Structural Statistics

NMR Restraints	
no. of distance restraints	
total	1708
intraresidue	160
sequential (i, $i+1$)	537
medium-range from (i, $i+2$) to (i, $i+5$)	640
long range (i, $i+5$)	371
no. of $M^{2+/3+}$ restraints	
total	13
I site	6
II site	7
H-bond	18
no. of dihedral angles	
total	110
ϕ	55
ψ	55
stereospecific assignments	31
no. of pseudocontact shift (PCS)	
total	142
backbone N	62
backbone HN	62
side chain N	6
side chain HN	12
no. of residual dipolar coupling (RDC)	
total	37
backbone	37
side chains	−
Structural Statistics[a]	
most favored region (%)	79.8
additional allowed region (%)	20.2
generously allowed region (%)	0
disallowed region (%)	0
no. of bad contacts/100 residues	0
H bond energy (kJ/mol)	3.63
overall *G*-factor	−0.27

[a] Values are for the minimized average structure. PROCHECK-NMR (*47*) was used to assess the overall quality of the structure. For the PROCHECK statistic, fewer than 10 bad contacts per 100 residues, an average hydrogen bond energy in the range of 2.5−4.0 kJ/mol and an overall *G*-factor of greater than −0.5 are expected for a good quality structure.

where χ, θ, and ω are the polar coordinates of the resonating nuclei.

A plot of the calculated versus experimental PCS values is given in the Supporting Information. PCS values used in solution structure calculations can also be found in the Supporting Information.

Residual Dipolar Couplings. RDC (*64*) are due to partial orientation of the molecules in the magnetic field due to anistropic susceptibility and are detected through ^1J measurements. The paramagnetic contributions to RDC for backbone amides were determined as a difference between the ^iJ measured in the Tb^{3+}-substituted derivative and those measured on the native protein.

The paramagnetic RDC^{para} are related to structural parameters through the following equation (*65*):

$$\mathrm{RDC}^{para} = -\frac{1}{4\pi}\frac{{B_0}^2}{15kT}\frac{\gamma_H\gamma_N h}{4\pi^2 r_{HN}^3}\left[\Delta\chi_{ax}^{para}(3\cos^2\theta - 1) + \frac{3}{2}\Delta\chi_{rh}^{para}(\sin^2\theta\cos 2\phi)\right] \quad (2)$$

where χ_{ax}^{para} is the axial and χ_{rh}^{para} the rhombic tensor parameter determined by the PCS (see above) while θ and

Table 2: Restraints Used in Structure Calculations Resulting in the Target Function and Mean rmsd Values for the Backbone and Heavy Atoms

		target function (Å^2)					mean rmsd (Å^2)[a,b]	
diamagnetic restraints	paramagnetic restraints	diamagnetic restraints	VdW[c]	PCS	RDC	total	backbone	heavy atoms
1714 NOEs, 44 H-bonds, 55 ψ angles, 55 ϕ angles	−	0.21	0.09			0.22 ± 0.03	0.59 ± 0.06	1.11 ± 0.09
1714 NOEs, 44 H-bonds, 55 ψ angles, 55 ϕ angles	142 PCS	0.14	0.12	0.13		0.40 ± 0.07	0.55 ± 0.09	1.09 ± 0.07
1714 NOEs, 44 H-bonds, 55 ψ angles, 55 ϕ angles	142 PCS, 37 RDC	0.16	0.17	0.38	0.02	0.73 ± 0.10	0.50 ± 0.09	1.09 ± 0.08

[a] For 20 structures. [b] Residues 3−108. [c] Target function for van der Waals violations.

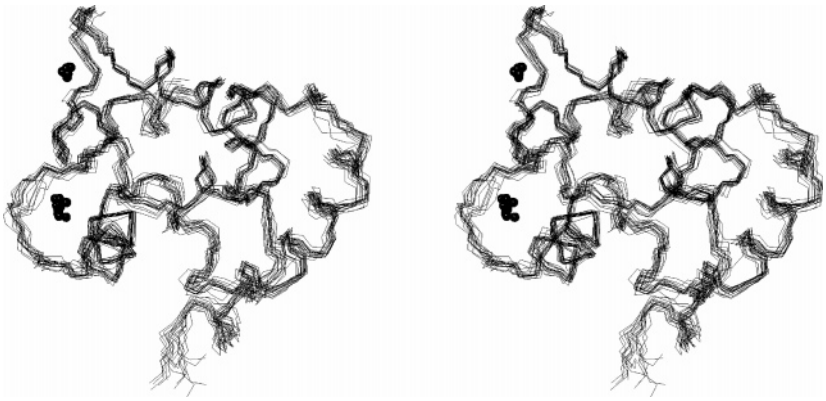

FIGURE 1: Stereoview of the final family of 20 conformers.

ϕ are the polar coordinates describing the N−H bond orientation within the principal axis system of the χ^{para} tensor. r_{NH} is the bond length between the H and N atoms. Other symbols have their usual meaning. RDC values of 37 NHs could be measured which were evenly distributed along the sequence, except the stretch of the Tb^{3+}-binding loop (residues 90−101). A plot of calculated versus experimental RDC values is given in the Supporting Information.

RDC values used in structure calculations for CaTbOM are also given in the Supporting Information. The final tensor parameters, after structure refinement, were $(39.6 \pm 0.8) \times 10^{-32}$ and $(5.7 \pm 0.8) \times 10^{-32}$ m^3.

In summary for the structure calculation, a total of 1708 meaningful NOEs, 55 ϕ and 55 ψ dihedral angles, 31 stereospecific proton pairs, 18 hydrogen bonds, 142 PCS, and 37 RDC (Table 1) were used in DYANA calculations using the PSEUDYANA module (*62*). Paramagnetic restraints improved the quality of the structure (Table 2) not only for the residues for which PCS or PCS and RDC values were available but also elsewhere. Particularly, all nonhelical parts were improved. The two calcium binding sites are quite improved, despite the fact that no restraints could be obtained in the immediate neighborhood of the paramagnetic metal. Also, a relevant improvement was obtained for helix 3. The mean rmsd values per residue for the two structure families calculated using diamagnetic restraints only and diamagnetic restraints with both PCS and RDC values are given in the Supporting Information. Figure 1 shows the final family of 20 conformers. For the average final structure, 79.8% of the residues are in most favored regions and 20.2% in additionally allowed regions of the Ramachandran plot (Table 1). These statistics demonstrate a good quality of the solution structure as confirmed by the fact that they do not substantially change using the RAMADYANA module (*48*).

Mobility Data. The NMR experiments for mobility data were performed at either 283 or 298 K using a 600 MHz spectrometer. The average R_1, R_2, and NOE values are consistent with a monomeric 12 kDa protein. The relaxation rates merely showed fluctuation along the sequence, showing that no regions are highly flexible. We did not notice a significant increase in mobility when the temperature was increased from 283 to 298 K.

DISCUSSION

Comparison with the Paralog Human α-Parvalbumin and Their Rat Orthologs. A detailed comparison between the 3D structure of human and rat OM, which is available at 1.3 Å resolution, showed a good agreement between the two structures, as expected. The two ortholog proteins in fact have a level of residue identity of 88%. Table 3 shows the sequence alignment for human and rat oncomodulins together with human and rat α-parvalbumins. A secondary structure comparison is also shown. The solution structure of human OM is characterized by the following secondary structure elements (residues in parentheses): α1 (2−4), α2 (7−17), α3 (26−32), α4 (40−50), β1 (57 and 58), α5 (60−63), α6 (64−69), α7 (79−89), β2 (97 and 98), and α8 (99−107). The secondary structure elements found are largely in agreement with the ones of the crystal structure of rat OM, as expected, with the only exception being helix 5, which starts one amino acid before and is immediately connected to helix 6, giving rise to a single-kink helix, while in the rat structure, the two helices are divided by a two-residue linker. The latter helices are separated by a short connecting linker also in the human and rat PV structure, as shown in Table 3.

Only few local differences are present. As previously done in the comparison of human and rat PV (*23*), the Ramachan-

Table 3: Sequence Alignment for Human and Rat Oncomodulin and Parvalbumin, as Well as a Comparison of the Secondary Structure and Ramachandran Region[a]

	10	20	30	40	50	60	70	80	90	100
H-OM	**MSITDVLSADD IAAALQECRD PDTFEPQKFF QTSGLSKMSA NQVKDVFRFI DNDQSGYLDE EELKFFLQKF ESGARELTES ETKSLMAAAD NDGDGKIGAE EFQEMVHS-**									
	CTHHHBTHHH HHHHHHHBCT BBCCTHHHHH HHBTCBBBTH HHHHHHHHHH TBBCCBSSTH HHHHHHHHHB TBBCTCBTHH HHHHHHHHHC BBBBBCSSHH HHHHHHHC									
	AAAAAAAAA AAAAAAAAAB BLABBAAAAA AAALAAABBA AAAAAAAAAA BAALALBBBA AAAAAAAAAA BAABAAABAA AAAAAAAAAB AALALBBBAA AAAAAA									
	10	20	30	40	50	60	70	80	90	100
R-OM	**SITDILSAED IAAALQECQD PDTFEPQKFF QTSGLSKMSA SQVKDIFRFI DNDQSGYLDG DELKYFLQKF QSDARELTES ETKSLMDAAD NDGDGKIGAD EFQEMVHS-**									
	THHHBBTHHH HHHHHHHBCT BBCCTHHHHH HHBTHHHBTH HHHHHHHHHH TBBCBBSSTT HHHHTTHHHB TBBBCCCTHH HHHHHHHHHC CBBBBBSSHH HHHHHHCC									
	AAAABBAAA AAAAAAAAAB BLABBAAAAA AAALAAABBA AAAAAAAAAA BAALALBBBL AAAAAAAAAA BAABBBBBAA AAAAAAAAAB AALALBBBAA AAAAAA									
	10	20	30	40	50	60	70	80	90	100
H-PV	**MSMTDLLNAED IKKAVGAFSA TDSFDHKKFF QMVGLKKKSA DDVKKVFHML DKDKSGFIEE DELGFILKGF SPDARDLSAK ETKMLMAAGD KDGDGKIGVD EFSTLVAES**									
	CTBTBBBTHHH HHHHHHHHCB BBCCTHHHHH HHBTHHHBTH HHHHHHHHHH TBBCBBSSTH HHHBTTHHHH TBBCCCCTHH HHHHHHHHHC BBBBBBSSHH HHHHHHHHC									
	BBAAAABAAA AAAAAAAABB AAABBAAAAA AAALAAABBA AAAAAAAAAA BAALALBBBA AAAAAAAAAA BBLABBBBAA AAAAAAAAAB AALALBBBAA AAAAAAAA									
	10	20	30	40	50	60	70	80	90	100
R-PV	**SMTDLLSAED IKKAIGAFTA ADSFDHKKFF QMVGLKKKSA DDVKKVFHIL DKDKSGFIEE DELGSILKGF SSDARDLSAK ETKTLMAAGD KDGDGKIGVE EFSTLVAES**									
	THHHHBTHHH HHHHHHTTCT BBCCTHHHHH HHHTHHHBTH HHHHHHHHHH TBBCBBSSTH HHHHTHHHHH TBBBCCCTHH HHHHHHHHHC BBCBBBSSHH HHHHHHHCC									
	AAAABBAAA AAAAAAAAAB BLABBAAAAA AAALAAABBA AAAAAAAAAA BAALALBBBA AAAAAAAAAA BAABBBBBAA AAAAAAAAAB AALALBBBAA AAAAAAAA									

[a] Symbols used for secondary structure comparison indicate the following: H for helix, S for β-sheet, C for coil, T for turn, and B for bend. Symbols used for the backbone angle comparison indicate the characteristic region of the Ramachandran plot (A, B, or L).

Table 4: Interhelix Angles and Distances for Human and Rat Oncomodulin and Parvalbumin[a]

PDB	AB	AC	AD	AE	AF	BC	BD	BE	BF	CD	CE	CF	DE	DF	EF	protein
								Interhelix Angles								
1rro	150.1	−59.6	−100.7	120.1	81.9	113.9	53.1	−83.0	−75.7	114.0	−144.0	116.1	101.6	−24.1	95.5	R-OM (1.3 Å)
honc	139.5	−69.6	−101.0	118.6	78.6	103.4	39.1	−94.0	−76.4	98.8	−137.1	129.1	118.4	−49.3	92.8	H-OM (NMR)
1rtp	152.8	−60.5	−107.7	118.2	81.2	109.8	50.9	−86.5	−81.7	113.0	−136.2	116.3	104.9	−31.5	104.0	R-PV (2.0 Å)
hprv	161.6	−48.7	−120.1	118.1	79.3	119.9	44.2	−79.9	−94.1	106.2	−140.6	109.1	110.6	−57.6	102.2	H-PV (NMR)
								Interhelix Distances								
1rro	9.4	18.2	20.3	19.4	20.3	15.5	18.8	14.1	13.0	16.3	19.4	10.2	11.1	16.7	13.8	R-OM (1.3 Å)
honc	10.1	18.3	20.7	17.2	20.2	15.5	18.8	12.3	12.4	16.2	18.8	10.1	10.6	16.0	14.0	H-OM (NMR)
1rtp	9.7	18.1	20.2	20.5	20.7	15.2	18.7	15.2	13.2	15.9	19.4	10.2	10.8	15.9	14.1	R-PV (2.0 Å)
hprv	8.7	15.8	19.9	19.0	17.9	14.5	19.8	15.7	11.2	16.9	19.9	11.1	10.3	17.6	14.6	H-PV (NMR)

[a] Angles and distances were calculated with interhlx (*66*). Sign convention is as described by Drohat et al. (*73*). Helix A consists of residues 10−17, helix B residues 26−32, helix C residues 40−50, helix D residues 60−63, helix E residues 79−89, and helix F residues 99−107.

dran values of each residue were analyzed for the two ortholog proteins (Table 3) to obtain information about these local but still important differences. By looking at these differences in detail, we find it is apparent that some residues are in different regions (e.g., from the A to the B region of the Ramachandran plane or vice versa) between the two ortholog proteins.

All the differences are related to residues located in loops: Leu 6, Ser 7, Arg 75, Glu 76, and Leu 77. In the case of Leu 6, which occurs before helix 2, the Ramachandran plot shows that the ϕ and ψ angles of this residue are in the A region, whereas those of rat OM are in the B region. In this case, the residues that immediately precede the sequence are different. In fact, for the human OM, we have a Val at position 5, while in the case of the rat, the residue preceding Leu 6 is an Ile. The same residue showed such differences in the Ramachandran values for the human α-PV as previously described (*23*). The following residue, Ser 7, exhibits the same behavior with ϕ and ψ dihedral angles characteristic of the A region in the Ramachandran plot for the human OM structure. An ADD stretch follows Ser 7 in the human OM, while an AED stretch follows in rat OM and both human and rat PVs.

A second difference between the two structures is observed at residues 75−77, which are in the linker connecting the CD and EF sites (residues 70−78). The ϕ and ψ angles place these residues in the A, A, and A regions, respectively, whereas those of the rat protein are in the B, B, and B regions, respectively.

Another difference is related to Glu 60, which is clearly in the A region and therefore is the starting residue of helix 6. The corresponding amino acid in rat OM is a Gly, and its ϕ and ψ angles are out of the allowed regions in the Ramachandran plot. A comparison with the two α-parvalbumins showed that residue 60, which is a Glu in both cases, is also placed in the A region of the Ramachandran plane.

In summary, there are three different regions in human OM, around Ser 7, Gly 60, and Arg 75, that show a distinct change, beyond uncertainty, in the local fold with respect to rat OM, and in each of these three cases, this difference is related to a difference in one amino acid between the two ortholog proteins.

A detailed comparison of interhelix angles and distances of OM with its ortholog and paralog proteins showed some small differences of a more global nature. The interhelix angles, calculated with the interhlx program (*66*) in Table 4, are defined between the two helix stretches closest to the AB, CD, and EF sites, and therefore involve helices α2 and α3, α4 and α5, and α7 and α8. The interhelix distances are measured between midpoints of the helices.

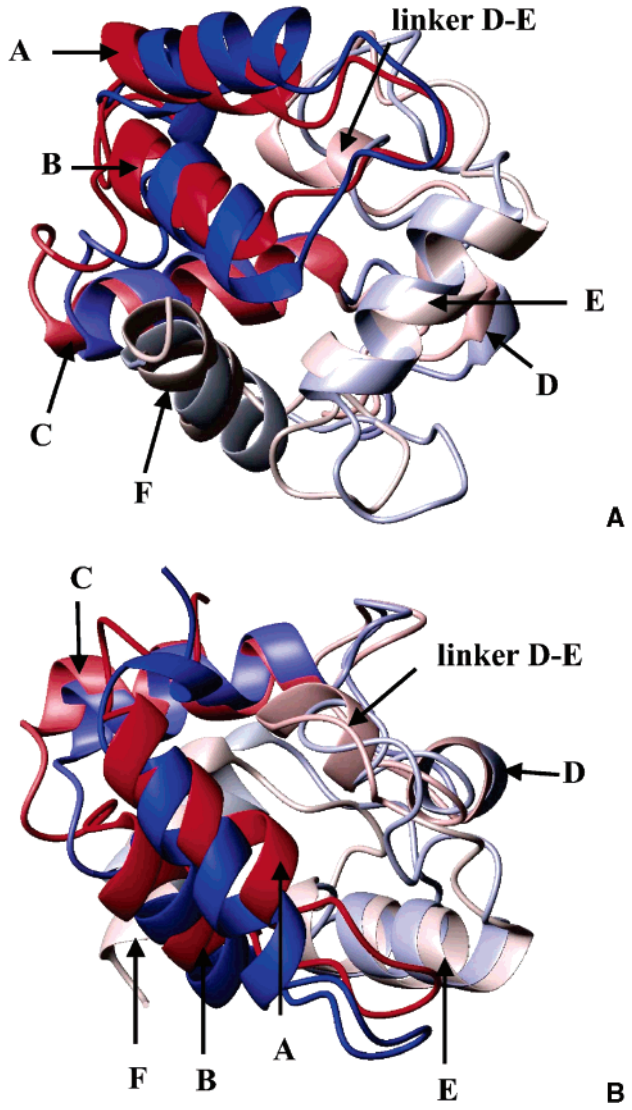

FIGURE 2: Superposition of calcium-loaded human oncomodulin (blue) and parvalbumin (red). The helix pairs are shown with different color intensities, becoming lighter going from the N-terminus (AB, dark) to the C-terminus (EF, light). In panel A, the molecules are oriented in such a way that the bottom of the "basket" formed by the C-terminal domain (EF-hands CD and EF) is at the bottom part of the figure and the basket "lid" constituted by helices A and B is at the top. In panel B, the molecules are rotated about the *x*-axis by 90°, relative to the orientation in panel A. From this perspective, the side shift of the AB domain with respect to the linker between helices D and E is evidenced.

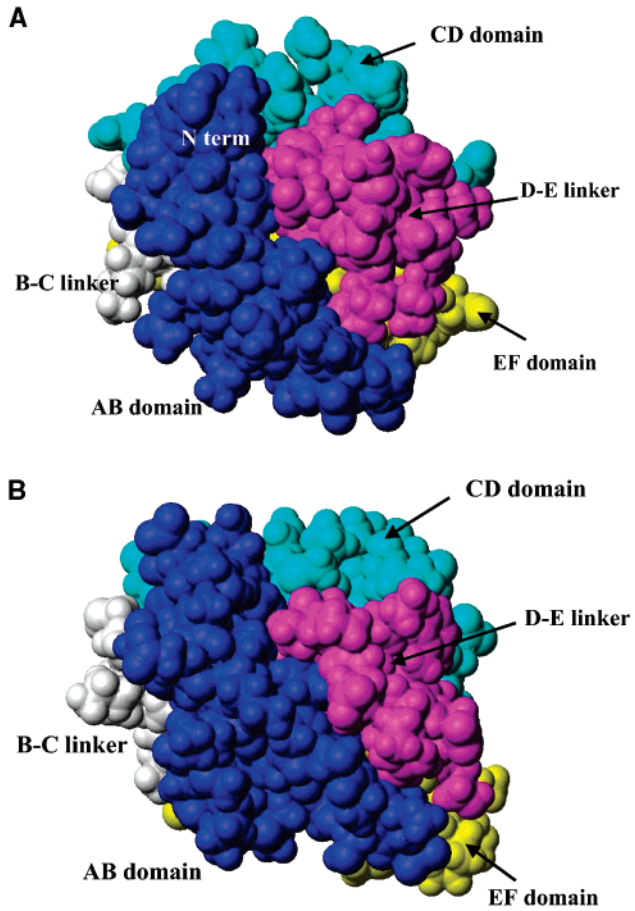

FIGURE 3: Surface representation (VdW radii) of human oncomodulin (A) and parvalbumin (B). The N-terminal AB domain (residues 1−33) is colored blue, the linker between helices B and C (residues 34−39) white, the CD EF-hand (residues 40−63) cyan, the linker between helices D and E (residues 64−78) magenta, and the C-terminal EF EF-hand (residues 79−108) yellow. The molecules have the same orientation, after best fit superposition of helices C−F. Note the poorer fit between the AB domain and the D−E linker in OM with respect to PV.

By first examining the functional C-terminal domain of all proteins (CD and EF sites), we keep the EF angle constant in both rat and human OM, being higher in PV, while the CD angle is much smaller in human OM than in rat OM, accentuating the trend already observed between human and rat PV. Much larger variations are found in the AB domain, since the AB angle differs by as much as 22° between human OM and PV. Interestingly, the same angle has an intermediate value in both rat proteins. The interhelical distances reflect the same difference between the human and rat protein.

Another feature that is worth noting is the variation in the AE interhelical distances. They are smaller in OM than in PV, and within each ortholog, they are smaller in the human than in the rat proteins. The BE interhelical distance is also shorter in human OM than in the other proteins. Overall, the AB site in OM (and particularly in human OM) is closer to the CD and EF sites than it is in PV. In Figure 2, the solution structures of the two Ca^{2+}-loaded human proteins are superimposed with MOLMOL (*46*). It is evident that while the CD and EF sites are very much coincident, the nonfunctional AB site is rather different in orientation in the two PVs. This geometrical difference can be described (Figure 2B) as a down-left movement of helix A in OM, which in turn pushes helix B toward helix F, the latter being forced toward the bottom of the CD−EF basket (Figure 2A).

Looking at the surface of the two proteins (Figure 3), we find that the overall result of such an extensive movement is the enlargement of the crevice located between the AB domain (blue) and the linker connecting helices D and E (magenta).

Inferences from the Structural Comparison. A comparison with Ca^{2+}-loaded EF-hand pairs III and IV of human calmodulin (CaM) shows that these two EF-hands have a structural arrangement that is very similar to those of the CD and EF sites of human OM and PV (Figure 4). The overall structural similarity between the two human PVs and with CaM is in line with the hypothesis that they share a common evolutionary ancestor endowed with the prototypical calmodulin-like structure of two EF-hand pairs separated by

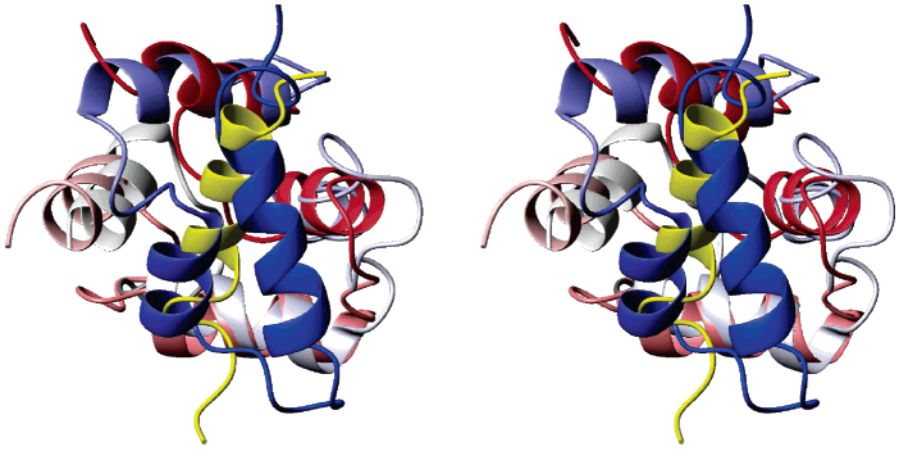

FIGURE 4: Superposition (stereoview) of human oncomodulin (blue) and the C-terminal domain of human calmodulin (red) bound to the C20W peptide (yellow) belonging to the N-terminal portion of the CaM-binding domain of the plasma membrane calcium pump. The helix pairs are shown with different color intensities, becoming lighter going from the N-terminus to the C-terminus. The superposition was obtained by best fitting the CD and EF domains of OM with the corresponding C-terminal sites III and IV of CaM. It appears that the endogenous AB domain of OM occupies a position very similar to that of the exogenous C20W peptide bound to CaM.

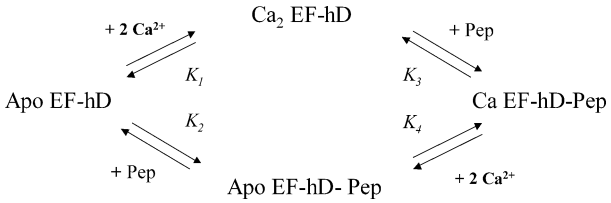

FIGURE 5: Thermodynamic cycle describing the binding to an apo EF-hand pair domain (Ef-hD) of two calcium ions and a target peptide, in whatever order. The higher affinity of the peptide for the calcium form ($K_3 \gg K_2$) implies a higher affinity of calcium for the apo EF-hand pair−peptide adduct ($K_4 \gg K_1$).

a linker. The presence in the m-RNA 5′-UTR of vertebrate α-PVs of a pseudocoding sequence for an EF-hand favors this possibility, by which a first evolutionary branching from the calmodulin-like ancestor was determined by the loss of the first EF-hand and the loss of Ca^{2+} binding ability of the second EF-hand, in an unknown order.

Given the strong similarity of the C-terminal halves of PVs, it is difficult to understand why the OM CD site is ∼1 order of magnitude less able to bind Ca^{2+} than the corresponding PV site (*14*). However, the observation described here of a different arrangement of the AB site with respect to the CD and EF sites may hint at a possible explanation. Calcium binding in CaM and other calcium sensor proteins is known to dramatically increase the affinity of one (or two) EF-hand pair(s) for a target peptide with respect to the corresponding calcium-free EF-hand pair. From a thermodynamic point of view, this is equivalent to stating that the presence of a bound target peptide increases the affinity for calcium of a calcium-free EF-hand pair. In Figure 5, a thermodynamic cycle describing the binding to an apo EF-hand pair domain (Ef-hD) of two calcium ions (assumed to be cooperative without a loss of generality) and a target peptide, in whatever order, is shown (*67*−*69*). As it is well-known that in a typical Ca^{2+}-activated EF-hand $K_3 \gg K_2$, it follows that $K_4 \gg K_1$; i.e., binding of calcium to an apo EF-hand is enhanced by the presence of a bound peptide. If we view the AB sites in α- and β-PVs as endogenous "target peptides", the high calcium affinity of parvalbumins is justified, and the *differences* in calcium affinity between the two proteins may be related to the different stability of the resulting "adduct". Indeed, upon removal of the AB loop in pike PV, the calcium affinity of the remaining CD−EF fragment decreases by 2 orders of magnitude (*70*), suggesting that evolution of the AB site to an abortive site was instrumental in the increase of the Ca^{2+} affinity of the CD−EF domain in PVs.

It is worth recalling that the level of sequence identity between the two proteins is 50%, but the conserved residues are differently distributed among EF-hand pairs. Indeed, the AB site has the lowest level of identity (44%), followed by the EF (50%) and CD (53%) pairs. Additionally, the loop between helices A and B shows an even larger variance: only two residues of eight are conserved, while four and eight of nine residues are conserved in the CD and EF loops, respectively.

It is possible, therefore, that given the intrinsic differences between the two AB sites, their "binding" to the rest of the protein is weaker in OM than it is in PV. Figure 3 suggests that the AB site, composed of helices A and B separated by the AB linker, is less engulfed in the hydrophobic pocket defined by the BC and DE linkers in OM (Figure 3A) than it is in PV (Figure 3B). Although less evident in the rat orthologs, the presence of a deeper surface pocket involving residue 18 was also pointed out.

Finally, it may be interesting to compare the arrangement of the AB site in the two proteins with those of target peptides that are known to bind to only the C-terminal domains of CaM (*71*) and myosin light chains (*72*), at variance with the classical peptide binding mode involving both N- and C-terminal domains. Figure 4 shows a superposition of human OM with the C-terminal domain of CaM bound to a peptide (C20W) belonging to the N-terminal portion of the CaM-binding domain of the plasma membrane calcium pump (*71*). After the EF-hand pairs are superimposed, the AB domain occupies a position similar to that of C20W, with the beginning of helix A being very close to the N-terminus of C20W and with helix B very close to its C-terminus.

SUPPORTING INFORMATION AVAILABLE

Acquisition parameters for NMR experiments; ^{1}H, ^{15}N, and ^{13}C resonance assignments; stereospecific assignments

and dihedral angle restraints; and pseudocontact shift and residual dipolar couplings used for structure refinement (Tables S1−S8). Figures S1−S4 are plots of the meaningful NOEs per residue, mean backbone rmsds per residue, calculated versus experimental PCS, and calculated versus experimental RDC, respectively. This material is available free of charge via the Internet at http://pubs.acs.org.

REFERENCES

1. Goodman, M., and Pechere, J. F. (1977) The evolution of muscular parvalbumins investigated by the maximum parsimony method, *J. Mol. Med. 9*, 131−158.
2. Stalker, J., Gibbins, B., Meidl, P., Smith, J., Spooner, W., Hotz, H. R., and Cox, A. V. (2004) The Ensembl Web Site: Mechanics of a Genome Browser, *Genome Res. 14*, 951−955.
3. Heizmann, C. W., Berchtold, M. W., and Rowsell, S. (1982) Correlation of parvalbumin concentration with relaxation speed in mammalian muscles, *Proc. Natl. Acad. Sci. U.S.A. 79*, 7243−7247.
4. Celio, M. R., and Heizmann, C. W. (1981) Calcium-binding protein parvalbumin as a neuronal marker, *Nature 293*, 300−302.
5. MacManus, J. P. (1979) Occurrence of a low-molecular-weight calcium-binding protein in neoplastic liver, *Cancer Res. 39*, 3000−3005.
6. Brewer, L. M., and MacManus, J. P. (1987) Detection of oncomodulin, an oncodevelopmental protein in human placenta and choriocarcinoma cell lines, *Placenta 8*, 341−363.
7. Durkin, J. P., Brewer, L. M., and MacManus, J. P. (1983) Occurrence of the tumor-specific, calcium-binding protein, oncomodulin, in virally transformed normal rat kidney cells, *Cancer Res. 43*, 5390−5394.
8. Bernaert, D., Brewer, L. M., MacManus, J. P., and Galand, P. (1989) Immunocytochemical detection of the onco-developmental protein oncomodulin in pre-neoplastic and neoplastic hepatocellular lesions during hepatocarcinogenesis in rats, *Int. J. Cancer 43*, 719−727.
9. Pfyffer, G. E., Haemmerli, G., and Heizmann, C. W. (1984) Calcium-binding proteins in human carcinoma cell lines, *Proc. Natl. Acad. Sci. U.S.A. 81*, 6632−6636.
10. Nestl, A., Von Stein, O. D., Zatloukal, K., Thies, W. G., Herrlich, P., Hofmann, M., and Sleeman, J. P. (2001) Gene expression patterns associated with the metastatic phenotype in rodent and human tumors, *Cancer Res. 61*, 1569−1577.
11. MacManus, J. P., Whitfield, J. F., and Stewart, D. J. (1984) The presence in human tumours of a Mr 11,700 calcium-binding protein similar to rodent oncomodulin, *Cancer Lett. 21*, 309−315.
12. Sakaguchi, N., Henzl, M. T., Thalmann, I., Thalmann, R., and Schulte, B. A. (1998) Oncomodulin is expressed exclusively by outer hair cells in the organ of Corti, *J. Histochem. Cytochem. 46*, 29−40.
13. Kretsinger, R. H., and Nockolds, C. E. (1973) Carp muscle calcium-binding protein. II. Structure determination and general description, *J. Biol. Chem. 248*, 3313−3326.
14. Wnuk, W., Cox, J. A., and Stein, E. A. (1982) in *Calcium & Cell Function* (Cheung, W.Y., Ed.) pp 243−278, Academic Press, New York.
15. McPhalen, C. A., Strynadka, N. C. J., and James, M. N. G. (1991) Calcium binding sites in proteins: A structural perspective, *Adv. Protein Chem. 42*, 77−144.
16. Moeschler, H. J., Schaer, J. J, and Cox, J. A. (1980) A thermodynamic analysis of the binding of calcium and magnesium ions to parvalbumin, *Eur. J. Biochem. 111*, 73−78.
17. Rinaldi, M. L., Haiech, J., Pavlovitch, J., Rizk, M., Ferraz, C., Derancourt, J., and Demaille, J. G. (1982) Isolation and characterization of a rat skin parvalbumin-like calcium-binding protein, *Biochemistry 21*, 4805−4810.
18. Eberhard, M., and Erne, P. (1994) Calcium and magnesium binding to rat parvalbumin, *Eur. J. Biochem. 222*, 21−26.
19. Cox, J. A., Milos, M., and MacManus, J. P. (1990) Calcium- and magnesium-binding properties of oncomodulin. Direct binding studies and microcalorimetry, *J. Biol. Chem. 265*, 6633−6637.
20. MacManus, J. P. (1981) The stimulation of cyclic nucleotide phosphodiesterase by a Mr 11500 calcium binding protein from hepatoma, *FEBS Lett. 126*, 245−249.
21. Boynton, A. L., MacManus, J. P., and Whitfield, J. F. (1982) Stimulation of liver cell DNA synthesis by oncomodulin, an MW 11500 calcium-binding protein from hepatoma, *Exp. Cell Res. 138*, 454−457.
22. Blum, J. K., and Berchtold, M. W. (1994) Calmodulin-like effect of oncomodulin on cell proliferation, *J. Cell. Physiol. 160*, 455−462.
23. Baig, I., Bertini, I., Del Bianco, C., Gupta, Y. K., Lee, Y.-M., Luchinat, C., and Quattrone, A. (2004) Paramagnetism-based refinement strategy for the solution structure of human α-parvalbumin, *Biochemistry 43*, 5562−5573.
24. Ahmed, F. R., Rose, D. R., Evans, S. V., Pippy, M. E., and To, R. (1993) Refinement of recombinant oncomodulin at 1.30 Å resolution, *J. Mol. Biol. 230*, 1216−1224.
25. McPhalen, C. A., Sielecki, A. R., Santarsiero, B. D., and James, M. N. (1994) Refined crystal structure of rat parvalbumin, a mammalian α-lineage parvalbumin, at 2.0 Å resolution, *J. Mol. Biol. 235*, 718−732.
26. Regeimbal, J., and Bardwell, C. A. (2002) DsbB Catalyzes Disulphide Bond Formation *de Novo*, *J. Biol. Chem. 277*, 32706−32713.
27. Schleucher, J., Schwendinger, M., Sattler, M., Schmidt, P., Schedletzky, O., Glaser, S. J., Sørensen, O. W., and Griesinger, C. (1994) A general enhancement scheme in heteronuclear multidimensional NMR employing pulsed field gradients, *J. Biomol. NMR 4*, 301−306.
28. Bertini, I., Janik, M. B. L., Lee, Y.-M., Luchinat, C., and Rosato, A. (2001) Magnetic Susceptibility Tensor Anisotropies for a Lanthanide Ion Series in a Fixed Protein Matrix, *J. Am. Chem. Soc. 123*, 4181−4188.
29. Piotto, M., Saudek, V., and Sklenar, V. (1992) Gradient-tailored excitation for single quantum NMR spectroscopy of aqueous solutions, *J. Biomol. NMR 2*, 661−666.
30. Delaglio, F., Grzesiek, S., Vuister, G., Zhu, G., Pfeifer, J., and Bax, A. (1995) NMRPipe: A multidimensional spectral processing system based on UNIX Pipes, *J. Biomol. NMR 6*, 277−293.
31. Goddard, T. D., and Kneller, D. G. (2000) *SPARKY 3*, University of California, San Francisco.
32. Tjandra, N., Grzesiek, S., and Bax, A. (1996) Magnetic field dependence of nitrogen-proton J splittings in ^{15}N-enriched human ubiquitin resulting from relaxation interference and residual dipolar coupling, *J. Am. Chem. Soc. 118*, 6264−6272.
33. Ottiger, M., Delaglio, F., and Bax, A. (1998) Measurement of J and dipolar couplings from simplified two-dimensional NMR spectra, *J. Magn. Reson. 131*, 373−378.
34. Grzesiek, S., and Bax, A. (1993) The importance of not saturating H_2O in protein NMR. Application to sensitivity enhancement and NOE measurements, *J. Am. Chem. Soc. 115*, 12593−12594.
35. Kay, L. E., Torchia, D. A., and Bax, A. (1989) Backbone dynamics of proteins as studied by ^{15}N inverse detected heteronuclear NMR spectroscopy: Application to staphylococcal nuclease, *Biochemistry 28*, 8972−8979.
36. Murthy, N. N., Karlin, K. D., Bertini, I., and Luchinat, C. (1997) NMR and electronic relaxation in paramagnetic dicopper(II) compounds, *J. Am. Chem. Soc. 119*, 2156−2162.
37. Marquardt, D. W. (1963) An algorithm for least-squares estimation of nonlinear parameters, *J. Soc. Ind. Appl. Math. 11*, 431−441.
38. Press, W. H., Flannery, B. P., Teukolsky, S. A., and Vetterling, W. T. (1988) in *Numerical Recipes in C: The Art of Scientific Computing*, Cambridge University Press, New York.
39. Palmer, A. G., III, Rance, M., and Wright, P. E. (1991) Intramolecular motions of a zinc finger DNA-binding domain Xfin characterized by proton-detected natural abundance ^{13}C heteronuclear NMR spectroscopy, *J. Am. Chem. Soc. 113*, 4371−4380.
40. Güntert, P., Braun, W., and Wüthrich, K. (1991) Efficient computation of three-dimensional protein structures in solution from nuclear magnetic resonance data using the program DIANA and the supporting programs CALIBA, HABAS and GLOMSA, *J. Mol. Biol. 217*, 517−530.
41. Güntert, P., Mumenthaler, C., and Wüthrich, K. (1997) Torsion Angle Dynamics for NMR Structure Calculation with the New Program DYANA, *J. Mol. Biol. 273*, 283−298.
42. Allegrozzi, M., Bertini, I., Janik, M. B. L., Lee, Y.-M., Liu, G., and Luchinat, C. (2000) Lanthanide induced pseudocontact shifts for solution structure refinements of macromolecules in shells up to 40 Å from the metal ion, *J. Am. Chem. Soc. 122*, 4154−4161.
43. Gochin, M. (2000) A high-resolution structure of a DNA-chromycin-Co(II) complex determined from pseudocontact shifts in nuclear magnetic resonance, *Struct. Folding Des. 8*, 441−452.

44. Bertini, I., Lee, Y.-M., Luchinat, C., Piccioli, M., and Poggi, L. (2001) Locating the metal ion in calcium-binding proteins by using cerium(III) as a probe, *ChemBioChem 2*, 550−558.
45. The source codes of the modules PSEUDYANA and RDCDYANA-ORIENT are available at www.postgenomicnmr.net. They are implemented in the program PARAMAGNETICDYANA, which can be obtained through www.postgenomicnmr.net by those who already have a licensed version of DYANA [ETH, Zurich, Switzerland; Güntert, P., Mumenthaler, C., and Wüthrich, K. (1997) *J. Mol. Biol. 273*, 283−298]. FANTASIAN can be freely downloaded from www.postgenomicnmr.net.
46. Koradi, R., Billeter, M., and Wüthrich, K. (1996) MOLMOL: A program for display and analysis of macromolecular structure, *J. Mol. Graphics 14*, 51−55.
47. Laskowski, R. A., MacArthur, M. W., Moss, D. S., and Thornton, J. M. (1993) PROCHECK: A program to check the stereochemical quality of protein structures, *J. Appl. Crystallogr. 26*, 283−291.
48. Bertini, I., Cavallaro, G., Luchinat, C., and Poli, I. (2003) A use of Ramachandran potentials in protein solution structure determinations, *J. Biomol. NMR 4*, 355−366.
49. Pearlman, D. A., Case, D. A., Caldwell, J. W., Ross, W. S., Cheatham, T. E., Ferguson, D. M., Seibel, G. L., Singh, U. C., Weiner, P. K., and Kollman, P. A. (1997) *AMBER 5.0*, University of California, San Francisco.
50. Kay, L. E., Ikura, M., Tschudin, R., and Bax, A. (1990) Three-Dimensional Triple-Resonance NMR Spectroscopy of Isotopically Enriched Proteins, *J. Magn. Reson. 89*, 496−514.
51. Wider, G., Neri, D., Otting, G., and Wüthrich, K. (1989) A Heteronuclear Three-Dimensional NMR Experiment for Measurements of Small Heteronuclear Coupling Constants in Biological Macromolecules, *J. Magn. Reson. 85*, 426−431.
52. Salzmann, M., Pervushin, K., Wider, G., Senn, H., and Wüthrich, K. (1998) TROSY in triple-resonance experiments: New perspectives for sequential NMR assignment of large proteins, *Proc. Natl. Acad. Sci. U.S.A. 95*, 13585−13590.
53. Gardner, K. H., Konrat, R., Rosen, M. K., and Kay, L. E. (1996) An (H)C(CO)NH-TOCSY pulse scheme for sequential assignment of protonated methyl groups in otherwise deuterated ^{15}N, ^{13}C-labeled proteins, *J. Biomol. NMR 8*, 351−356.
54. Kay, L. E., Xu, G. Y., Singer, A. U., Muhandiram, D. R., and Forman-Kay, J. D. (1993) A gradient-enhanced HCCH-TOCSY experiment for recording side-chains ^{1}H and ^{13}C correlations in H_2O samples of proteins, *J. Magn. Reson., Ser. B 101*, 333−337.
55. Wider, G., Macura, S., Kumar, A., Ernst, R. R., and Wüthrich, K. (1984) Homonuclear Two-Dimensional ^{1}H NMR of Proteins. Experimental Procedures, *J. Magn. Reson. 56*, 207−234.
56. Wishart, D. S., and Sykes, B. D. (1994) The ^{13}C chemical shift index: A simple method for the identification of protein secondary structure using ^{13}C chemical shift data, *J. Biomol. NMR 4*, 171−180.
57. Kuboniwa, H., Grzesiek, S., Delaglio, F., and Bax, A. (1994) Measurements of HN−Ha *J* couplings in calcium-free calmodulin using 2D and 3D water flip-back methods, *J. Biomol. NMR 4*, 871−878.
58. Sykes, B. D., and Lee, L. (1983) Use of lanthanide-induced nuclear magnetic resonance shifts for determination of protein structure in solution: EF calcium binding site of carp parvalbumin, *Biochemistry 22*, 4366−4373.
59. Capozzi, F., Cremonini, M. A., Luchinat, C., and Sola, M. (1993) Assignment of pseudo-contact-shifted ^{1}H NMR resonances in the EF-site of Yb^{3+}-substituted rabbit parvalbumin through a combination of 2D techniques and magnetic susceptibility tensor determination, *Magn. Reson. Chem. 31*, S118−S127.
60. Allegrozzi, M., Bertini, I., Choi, S.-N., Lee, Y.-M., and Luchinat, C. (2002) Detecting small structural changes in metalloproteins by the use of NMR pseudocontact shifts, *Eur. J. Inorg. Chem.*, 2121−2127.
61. Herzberg, O., and James, M. N. (1986) Crystallographic determination of lanthanide ion binding to troponin C, *FEBS Lett. 199*, 279−281.
62. Banci, L., Bertini, I., Gori Savellini, G., Romagnoli, A., Turano, P., Cremonini, M. A., Luchinat, C., and Gray, H. B. (1997) The pseudocontact shifts as constraints for energy minimization and molecular dynamic calculations on solution structures of paramagnetic metalloproteins, *Proteins: Struct., Funct., Genet. 29*, 68−76.
63. Klingenberg, M. (1981) Membrane protein oligomeric structure and transport function, *Nature 290*, 449−454.
64. Tolman, J. R., Flanagan, J. M., Kennedy, M. A., and Prestegard, J. H. (1995) Nuclear magnetic dipole interactions in field-oriented proteins: Information for structure determination in solution, *Proc. Natl. Acad. Sci. U.S.A. 92*, 9279−9283.
65. Barbieri, R., Bertini, I., Cavallaro, G., Lee, Y.-M., Luchinat, C., and Rosato, A. (2002) Paramagnetically induced residual dipolar couplings for solution structure determination of lanthanide-binding proteins, *J. Am. Chem. Soc. 124*, 5581−5587.
66. Yap, K. L., Ames, J. B., Swindells, M. B., and Ikura, M. (2002) Vector Geometry Mapping: A method to characterize the conformation of helix-loop-helix calcium binding proteins, *Methods Mol. Biol. 173*, 324.
67. Peersen, O. B., Madsen, T. S., and Falke, J. J. (1997) Intermolecular tuning of calmodulin by target peptides and proteins: Differential effects on Ca^{2+} binding and implications for kinase activation, *Protein Sci. 6*, 794−807.
68. Brown, S. E., Martin, S. R., and Bayley, P. M. (1997) Kinetic control of the dissociation pathway of calmodulin-peptide complexes, *J. Biol. Chem. 272*, 3389−3397.
69. Mirzoeva, S., Weigand, S., Lukas, T. J., Shuvalova, L., Anderson, W. F., Watts, A., and Watterson, D. M. (1999) Analysis of the functional coupling between calmodulin's calcium binding and peptide recognition properties, *Biochemistry 38*, 3936−3947.
70. Maximov, E. E., and Mytin, I. V (1979) Binding of calcium by fragment 38−108 of pike parvalbumin, *Biochemie 61*, 751−754.
71. Elshorst, B., Hennig, M., Forsterling, H., Diener, A., Maurer, M., Schulte, P., Schwalbe, H., Griesinger, C., Krebs, J. F., Schmid, H., and Carafoli, E. (1999) NMR solution structure of a complex of calmodulin with a binding peptide of the Ca^{2+} pump, *Biochemistry 38*, 12320−12332.
72. Himmel, D. M., Gourinath, S., Reshetnikova, L., Shen, Y., Szent-Gyorgyi, A. G., and Cohen, C. (2002) Crystallographic Findings on the Internally Uncoupled and Near-Rigor States of Myosin: Further Insights Into the Mechanics of the Motor, *Proc. Natl. Acad. Sci. U.S.A. 99*, 12645.
73. Drohat, A. C., Baldisseri, D. M., Rustandi, R. R., and Weber, D. J. (1998) Solution structure of Calcium-bound rat S100B(bb) as determined by nuclear magnetic resonance spectroscopy, *Biochemistry 37*, 2729−2740.

BI048388O